RSC Advances

ROYAL SOCIETY OF CHEMISTRY

www.rsc.org/advances

Progress in Low Voltage Reversible Electrowetting with Lubricated Polymer Honeycomb Substrates

Edward Bormashenko[a,b], Roman Pogreb[a], Yelena Bormashenko[a], Hadas Aharoni,[b] Evgeny Shulzinger[a], Roman Grinev[a], Daniel Rozenman,[b] Ziva Rozenman.[b]

[a]*Ariel University, Physics Faculty, 40700, P.O.B. 3, Ariel, Israel*

[b]*Department of Chemical Engineering and Biotechnology, Ariel University, P.O.B. 3, Ariel 40700, Israel*

Low-voltage electrowetting on liquid infused films realized with lubricated honeycomb polymer surfaces is reported. Introduction of ethylene carbonate into the polymer (polycarbonate) matrix allowed an increase in the sensitivity of the scheme. A theoretical analysis of the thermodynamics of the electrowetting on liquid infused film is reported. Fitting of experimental data to theoretical curves allowed an estimation of the specific capacity of the double layer. An analysis of the viscous dissipation taking place under the proposed electrowetting scheme is presented.

Introduction

An interest in the phenomenon of electrowetting was boosted in the 1980s in the context of various applications of the effect, including lab-on-chip systems[1-4] and adaptive optical lenses.[1-7] Electrowetting is already coming to fruition for many applications, such as display technologies, droplet transport, smart optics, flexible systems, remote switching, electronic paper, miniaturized chemistry and energy harvesting.[8] Numerous applications of electrowetting were summarized in recent reviews.[8-10] However, the applications of electrowetting face a serious problem: the voltages necessary for manifestations of this effect are relatively high, on the order of magnitude of several hundred volts.[9-10] The important factor which adversely affects electrowetting is the effect of the pinning of the triple line, leading to high voltages

necessary for electrical actuation of droplets.[11] One of the most popular modern configurations of electrowetting experiments is the so-called electrowetting-on-dielectric scheme (EWOD), in which liquid is placed on an insulating layer on top of bare electrodes.[12-14] A detailed theoretical analysis of the EWOD scheme was undertaken recently in Refs. 14-15. A number of groups reported low-voltage EWOD schemes[16-23], exploiting a diversity of supporting dielectrics, including amorphous fluoropolymers,[16] solid-like ionic liquids,[17] parylene,[21] etc.

However, the EWOD scheme also suffers from the effect of the pinning of the triple line.[11] It was demonstrated recently that the impact of pinning may be essentially decreased when liquids are used as the dielectric layer.[24-25] Wang et al. coined for this scenario of electrowetting the abbreviation EWOLF, which means electrowetting on liquid-infused film.[25] Our paper is devoted to the further development of a low-voltage EWOLF scheme, enabling an essential decrease in the voltage necessary for the onset of electrical actuation of droplets.

Experimental

The EWOLF scheme was realized by the use of aluminum planar electrodes, coated with honeycomb composite films comprised of Polycarbonate (PC) and Ethylene Carbonate (EC). Composite films were deposited on the electrodes by the fast dip-coating process, as depicted in Figs. 1a-b. The fast dip-coating process is described in detail in Refs. 26-27. The solution used for the fast dip-coating contained: 84.15 wt.% of Dichloromethane (CH_2Cl_2), 10.11 wt.% of Chloroform ($CHCl_3$), 3.9 wt% of PC and 1.83 wt.% of EC. The higher concentrations of EC led to formation of defective micro-porous structures. The fast dip-coating carried out under the relative humidity (RH) of 40-50% gave rise to the "breath-figures" self-assembly,

reviewed recently in Refs. 28-30. PC is distinguished by its high dielectric constant ($\mathcal{E}$ =2.9) and dielectric strength (150 kV/cm).

A typical self-assembly pattern resulting from the breath-figures self-assembly, formed on aluminum plates, is depicted in Fig. 2. The average radius of pores was about 1.5 μm. The average depth of pores as established by AFM was about 1 μm. PC porous coatings were impregnated by the polydimethylsiloxane (PDMS) oil for MP&BP apparatus, for brevity called hereafter "silicone oil" (supplied by Sigma-Aldrich). This kind of oil was chosen due to its high dielectric strength (120 kV/cm) and low viscosity ($\eta_{oil} \cong 5\times10^{-2}$ Pa·s). For the purpose of uniform spreading of the oil, the lubricated substrates were heated to 60°C, and afterwards cooled to ambient temperature. The thickness of the oil layer was established by weighing as $l \cong 20 \pm 2$ μm(see Fig. 1b), which is much larger than the depth of the pores. The physical properties of the silicone oil relevant to our study are summarized in Table 1. Experiments were carried out with 8 μl bi-distilled water droplets. Droplets were visualized with a Ramé-Hart Advanced Goniometer, Model 500-F.

The surface tension of the silicone oil was established by the pendant drop method with a Ramé-Hart Advanced Goniometer, Model 500-F.

Theoretical analysis of the EWOLF electrowetting scheme.

In the EWOLF scheme, a water droplet is deposited on the oil layer.[24-25] The wetting regime is governed by the spreading parameter *S*, given by:

$$S = \gamma - (\gamma_{oil} + \gamma_{oil/water}), \qquad (1)$$

where $\gamma = 71\frac{mJ}{m^2}$, $\gamma_{oil} = 21\frac{mJ}{m^2}$ and $\gamma_{oil/water} = 23-24\frac{mJ}{m^2}$ are interfacial tensions at the water/vapor, oil/vapor and oil/water interfaces respectively (γ_{oil} was established experimentally as described in the experimental section; $\gamma_{oil/water}$ was extracted from the literature data[31]). Substituting the aforementioned values in Exp. 1, we obtain $S > 0$; in this case, the silicone oil is expected to coat the water droplet.[24, 32-34] Indeed,

the formation of the silicone oil layer coating the droplet was observed experimentally.

Thus, the actual wetting regime displayed schematically in Fig. 1a, illustrated in Fig. 3, and discussed recently in detail in Refs. 33-35, is rather intricate. The situation is complicated by the "wetting ridges" formed in the vicinity of the contact line, discussed in Refs. 33-34 and shown schematically in Fig. 3. The complicated shape of the water/vapor interface, exhibiting a flex point, is noteworthy, making an accurate measurement and interpretation of the contact angle quite challenging. For the analysis of the wetting situation, we implemented the following experimental procedure. We experimentally established the contact diameter 2*a* changing with a voltage *U* by means of a traditional goniometric procedure, and we interpreted the dependence *a(U)*, as will be discussed below.

Consider the free energy *G* of a water droplet deposited on the silicone layer and exposed to the voltage *U*, as described in Figs. 1a-b, 3 (the energy of the "wetting ridge" is neglected) :

$$G[h(x,y)] = \iint_S \left[(\gamma_{oil} + \gamma_{oil/water} + P(e)) \sqrt{(1+(\nabla h)^2} + (\gamma^*_{oil/water}(U) - \gamma_{oil}) \right] dxdy \,, \qquad (2)$$

where $\gamma^*_{oil/water}(U)$ is the surface energy of the oil/water interface exposed to voltage *U, e* is the thickness of the PDMS liquid layer coating a water droplet (see Fig. 3), $h(x,y)$ is the local height of the liquid surface above the point (x,y) of the substrate (it is supposed latently that there is no difference between surface tensions and surface energies for γ_{oil} , $\gamma_{oil/water}$), and the integral is extended over the wetted substrate area. The first term of the integrand presents the capillary energy of the liquid "composite" cap. It should be stressed that this energy is not modified by voltage. The second term describes the change in the energy of the oil/water interface modified by voltage, and it is usually related to the formation of the Helmholtz double layer.[10, 36-38] $P(e)$ is the term resulting from the disjoining pressure $\Pi(e)$ (see Refs. 36-39).

$$\Pi(e) = -\frac{dP}{de} \quad . \qquad (3)$$

Gravity is neglected, because it has no influence on the apparent contact angle (abbreviated APCA).[39] If we restrict ourselves to an axially symmetric "coated" droplet (shown in Fig. 3), the free energy *G* is given by the following expression:

$$G(h,h') = \int_o^a \left[2\pi(\gamma_{oil} + \gamma_{oil/water} + P(e))x\sqrt{1+h'^2} + 2\pi x(\gamma^*_{oil/water}(U) - \gamma_{oil})\right]dx , \quad (4)$$

where a is the contact radius of the droplet (see Fig. 3). We also suppose that the PDMS coated water droplet does not evaporate (this assumption is well-justified, because PDMS actually does not evaporate); thus, the condition of the constant volume V should be considered as:

$$V = \int_o^a 2\pi x h(x)dx = \text{const} . \quad (5)$$

It should be stressed that in the discussed experimental situation, where a water droplet is coated with oil, the volume of the droplet is constant.

Thus, the problem is reduced to the minimization of the functional:

$$G(h,h') = \int_0^a \widetilde{G}(h,h',x)dx , \quad (6a)$$

$$\widetilde{G}(h,h',x) = 2\pi(\gamma_{oil} + \gamma_{oil/water} + P(e))x\sqrt{1+h'^2} + 2\pi x(\gamma^*_{oil/water}(U) - \gamma_{oil}) + 2\pi\lambda x h , \quad (6b)$$

where λ is the Lagrange multiplier to be deduced from Exp. 5. If the endpoints of the contact line are free to move, the transversality condition at the endpoint a yields:[40]

$$(\widetilde{G} - h'\widetilde{G}'_{h'})_{x=a} = 0 , \quad (7)$$

where $\widetilde{G}'_{h'}$ denotes the h' derivative of $\widetilde{G}$. The procedure, described in detail in Ref. 39, yields for the apparent contact angle:

$$\cos\theta^* = \frac{\gamma_{oil} - \gamma^*_{oil/water}(U)}{\gamma_{oil} + \gamma_{oil/water} + P(e)} . \quad (8)$$

It is plausible to suggest that the change in the oil/water interfacial tension due to the voltage U is (as it occurs for solid dielectrics[10,36,38]) is described by:

$$\gamma^*_{oil/water}(U) = \gamma_{oil/water} - \frac{CU^2}{2} , \quad (9)$$

where C is the specific capacity of the double layer, which is inherent to the EWOLF scheme.[8-10] The thermodynamic justification of Eq. 9 is presented in Ref. 41. Substituting Exp. 9 into Exp. 8, and considering $\cos\theta = \frac{\gamma_{oil} - \gamma_{oil/water}}{\gamma_{oil} + \gamma_{oil/water} + P(e)}$ (where θ is the equilibrium contact angle of the system corresponding to the zero voltage situation[35]) results in the following expressions:

$$\cos\theta^* = \cos\theta + \frac{CU^2}{2(\gamma_{oil} + \gamma_{oil/water} + P(e))} = \cos\theta + \alpha U^2, \quad (10a)$$

$$\alpha = \frac{C}{2(\gamma_{oil} + \gamma_{oil/water} + P(e))} \quad , \quad (10b)$$

resembling the well-known Lippmann equation of electrowetting.[10, 32, 42-43] Exp. 10 leads to the expectable conclusion: the high sensitivity of the EWOLF scheme calls for high specific capacities *C*. Thus, a low-voltage EWOLF scheme should fulfill two main demands: low contact angle hysteresis,[11, 44-45] and the highest possible specific capacitances of the double layer *C*.

The first demand is fulfilled due to the fact that polymer substrates impregnated by oils demonstrate very low contact angle hysteresis.[24-25,33-34,46-52] Further progress in the development of low-voltage schemes may be obtained by increasing the specific capacitance *C*. For this purpose, ethylene carbonate (EC) was introduced into the PC matrix. The molecule of EC is characterized by an abnormally high molecular dipole moment of 4.9 D, leading to a dielectric constant as high as 90.[53-54] Thus, an essential increase in the specific capacity *C* results in a decrease of the voltage necessary for electrowetting actuation of droplets. It should be stressed that in our experiments, water soluble EC is isolated from water by the layer of PDMS, as depicted in Fig. 1.

Experimental results

We established that PC+EC silicone oil-impregnated honeycomb surfaces demonstrated low-voltage DC electrowetting, illustrated by Figs. 4-6. Fig. 4 depicts the distortion of the water droplet under applied voltage. Wetting ridges formed in the vicinity of the triple line are clearly seen.[33-34] The presence of wetting ridges makes accurate measurement of the apparent contact angles predicted by Exp. 10

problematic, due to the complicated shape of the water/vapor interface, exhibiting a flex point.

At the same time, the relative maximal displacement of the triple line $\Delta a / a_0$ may be accurately established experimentally with a goniometer. Fig. 5 depicts the dependence of the relative maximal displacement of the triple line as a function of the applied voltage *U*.

It is recognized from the data, displayed in Fig. 5, that the onset of the displacement of the triple line starts at the voltage of U_0=5 V. This voltage is markedly lower than the voltages reported in Refs. 24-25, and it is reasonable to relate the progress in the decrease of the voltage necessary for electrowetting actuation of droplets to the essential increase in the specific capacity of the scheme, achieved by introducing EC into the polymer matrix. The EWOLF scheme remained reversible up to threshold voltages of 50V.

It is reasonable to quantify the sensitivity of the EWOLF scheme by the parameter $\xi = \Delta a / a_0 U$, as proposed in Ref. 24. It is recognized from the experimental data that $\xi \cong 3.6 \times 10^{-3}\ \mathrm{V}^{-1}$ for the EWOLF scheme exploiting PC+EC silicone oil-impregnated honeycomb surfaces, which is markedly larger than that reported in Ref. 24 for pure PC substrates ($\xi \cong 1.3 \cdot 10^{-3}\ \mathrm{V}^{-1}$). This means that the presented scheme is more sensitive to the voltage than that reported in our previous paper.

The essential improvement of the sensitivity of the electrowetting scheme is reasonably related to the increase of the dielectric constant of the double layer stipulated by the introduction of EC, resulting in an increase in the specific capacity appearing in Ref. 10. However, the quantitative analysis of the experimental data is far from trivial. Indeed, Exps. 10a-b predict the apparent contact angle, whereas the

experimental procedure allows accurate establishment of the relative maximal displacement of the triple line $\Delta a / a_0$. Assuming that the droplet exposed to voltage keeps the shape of a spherical cap, accepting the constancy of the droplet's volume V and applying the well-known geometrical relations, supplied by Exps. 11a-b:

$$V = \frac{\pi}{3} R^3 (1-\cos\theta)^2 (2+\cos\theta) \qquad (11a)$$

$$a = R\sin\theta \ , \qquad (11b)$$

(where R is the radius of a droplet), yields the following expression for the relative maximal displacement of the triple line, yields the following:

$$\Delta a / a_0 = \left(\frac{1-\cos\theta}{1-\cos\theta^*}\right)^{\frac{2}{3}} \left(\frac{2+\cos\theta}{2+\cos\theta^*}\right)^{\frac{1}{3}} \frac{\sin\theta^*}{\sin\theta} - 1 . \qquad (12)$$

Fitting of the experimental data by the cumbersome function supplied by Exps. 10, 12 is presented in Fig. 5. The value of α (see Exp. 10b) was considered a fitting parameter. The best possible fitting (carried out with Origin 8.1 software) was obtained for $\alpha \cong 6\times 10^{-5} V^{-2}$. This makes possible a rough estimation of the specific capacitance of the double layer C. Indeed, if the effects due to the disjoining pressure are negligible, we have:

$$C \cong 2\alpha(\gamma_{oil} + \gamma_{oil/water}) \ . \qquad (13)$$

Substituting the abovementioned values of α, γ_{oil} and $\gamma_{oil/water}$ into Exp. 3 yields: $C \cong 5\frac{\mu F}{m^2}$. This value is smaller than the specific capacitances reported for EWOD schemes[55-56] and typical specific capacities inherent for double layers,[37] and this discrepancy calls for future investigations.

It should be emphasized that fitting of experimental data by Exp. 12 is possible only at the initial section of the experimental curve, i.e. at relatively low

voltages. At higher voltages of 100 V, the effect of saturation of the contact angle was observed, which is still not understood to its full extent.[57]

The dynamics of the EWOLF scheme.

When the triple line is displaced, viscous dissipation occurs in the water droplet and also within the oil layer. Both of the viscous dissipations (accurately speaking, the velocities of the viscous dissipations) are given by Exp. 14 (see Ref. 58):

$$\frac{dE_{visc}}{dt} = \eta \int_{V_d} (\nabla \vec{u})^2 dV \,. \qquad (14)$$

Here V_d is the volume over which viscous dissipation occurs, η is the viscosity of the liquid, and $\vec{u}$ is the velocity field in the liquid.[58] Assuming $(\nabla \vec{u})^2 \cong \left(\frac{\partial u}{\partial y}\right)^2$ (y is the vertical axis), we have for the viscous dissipation in the droplet $\frac{dE_{water}}{dt}$ (recall that the volume of the spherical segment is given by: $V = \pi H^2 (a - \frac{1}{3} H)$, a is the contact radius, and H is the height of a spherical segment, shown in Fig. 3):

$$\frac{dE_{water}}{dt} = \eta_{water} \int_{V_d} \left(\frac{\partial u}{\partial y}\right)^2 dV \cong \eta_{water} \frac{u^2}{H^2} \pi H^2 (a - \frac{1}{3} H) = \pi \eta_{water} u^2 (a - \frac{1}{3} H) \,. \qquad (15)$$

For the viscous dissipation $\frac{dE_{oil}}{dt}$ taking place within the oil layer, we have:

$$\frac{dE_{oil}}{dt} = \eta_{oil} \int_{V_d} \left(\frac{\partial u}{\partial y}\right)^2 dV \cong \eta_{oil} \frac{u^2}{l^2} \pi a^2 l = \pi \eta_{oil} u^2 \frac{a^2}{l} \,, \qquad (16)$$

where l is the thickness of the silicone oil layer, shown in Fig. 1b. Combining Exps. 15-16 yields:

$$\frac{E_{water}}{E_{oil}} \cong \frac{\eta_{water}}{\eta_{oil}} \frac{(a - \frac{1}{3} H) l}{a^2} \,. \qquad (17)$$

In our experiments $a \cong H$ takes place; this assumption gives rise to the following simple estimation:

$$\frac{E_{water}}{E_{oil}} \cong \frac{\eta_{water}}{\eta_{oil}} \frac{l}{a}. \quad (18)$$

In our experiments: $\eta_{oil} \cong 5\times10^{-2}\, Pa\times s; \eta_{water} \cong 10^{-3}\, Pa\times s; l \cong 20\times10^{-6} m; a \cong 10^{-3} m$.

Thus, we obtain: $\frac{E_{water}}{E_{oil}} \cong \frac{10^{-3}}{5\times10^{-2}} \frac{20\times10^{-6}}{10^{-3}} = 4\times10^{-4}$. This means, that in our experiments, the viscous dissipation is totally governed by the dissipation occurring in the silicone oil layer. In our estimation, we assumed that the thickness of the silicone oil layer is close to its initial value. However, the thickness of the oil layer essentially changes after loading a water droplet on its surface; it may be as low as 20 nm.[59] Considering this observation strengthens the conclusion that the viscous dissipation is controlled by the processes taking place in the oil layer.

The balance of interfacial and viscous forces acting within the silicone oil layer yields (see Ref. 18):

$$v \cong \frac{2l\Delta\gamma(U)}{\eta_{oil} a} \quad , \quad (19)$$

where v is the velocity of the triple line, and $\Delta\gamma(U)$ is the non-equilibrium, specific interfacial force depending on the applied voltage U. Combining Exps. 19 and 9 results in the following "naive" scaling law: $v \sim U^2$. The experimental dependence of the velocity of the triple line v on the applied voltage U is depicted in Fig. 6. The double logarithmic plot, $\ln v$ vs. $\ln U$ (presented in Fig. 6) is reasonably fitted with a straight line with a slope in the range of 1.8-2.2, supporting the square scaling law resulting from Exps. 19 and 9.

The further progress in the improvement of the sensitivity of the EWOLF scheme may be related to the increasing of the specific capacity C, exploiting of extremely low viscosity oils (see Eq. 19) and improvement of the polymer layer, preventing the charge leakage, as discussed in Ref. 60.

Conclusions

We conclude that impregnated porous polymer substrates demonstrate a potential for low-voltage electrowetting. Electrowetting on liquid-infused films allows low-voltage actuation of droplets, due to the low contact angle hysteresis inherent for liquid/liquid interfaces. We reported that introducing Ethylene Carbonate, (characterized by a very high dielectric constant) into the porous polymer film

enabled an increase of the sensitivity of the electrowetting scheme to the applied voltage. Voltages as low as 5V gave rise to the onset of displacement of the contact line. It is reasonable to relate the high sensitivity of the reported electrowetting scheme to the high specific capacity of the Helmholtz double layer. A theoretical analysis of the electrowetting on a liquid-infused polymer film was reported. An explicit equation predicting the apparent contact angle was derived. The specific capacity of the double layer *C* was calculated. The dynamics of the EWOLF scheme was analyzed. The viscous dissipation occurring under EWOLF is controlled by the processes taking place in the oil layer.

Acknowledgements

The Authors are grateful to Professor Gene Whyman for extremely fruitful discussions. The Authors are thankful to Mrs. Albina Musin for her inestimable help in preparing this manuscript, and to Mrs. Natalya Litvak for her kind help in SEM imaging.

References

1. S. K. Cho, H. J. Moon and C. J. Kim, *J. Microelectromech. Syst*. 2003, **12,** 70-80.
2. M. G. Pollack, R. B. Fair and A. D. Shenderov, *Appl. Phys. Lett*. 2000, **77**, 1725.
3. V. Srinivasan, V. K. Pamula and R. B. Fair, *Lab Chip* 2004, **4**, 310-315.
4. R. B. Fair, *Microfluidics and Nanofluidics* 2007, **3**, 245-281.
5. B. Berge and J. Peseux, *Europ. Phys. J. E* 2000, **3**, 159-163.
6. S. Kuiper and B. H. W. Hendriks, *Appl. Phys. Lett*. 2004, **85**, 1128-1130.
7. B. H. W. Hendriks and S. Kuiper, M. A. J. van As, C. A. Renders and T. W. Tukker, *Optical Review*, 2005, **12**, 255-259.
8. S. Arscott, *RSC Adv*., 2014, **4**, 29223-29238.
9. W. C. Nelson and C. J. Kim, *J. Adhesion Sci. Techn*. 2012, **26**, 1747-1771.
10. L. Chen and E. Bonaccurso, *Adv. Colloid Interface Sci*. 2013, **210**, 2-12.
11. R. Gupta, D. M. Sheth, T. K. Boone, A. B. Sevilla and J. Frechette, *Langmuir* 2011, **27**, 14923–14929.
12. B. Berge, *C. R. Acad. Sci. Paris* 1993, **317**, 157-163.
13. I. Moon and J. Kim, *Sensors Actuators A* 2006, **130–131**, 537-544.
14. W. Da and Y.-P. Zhao, *Int. J. Nonlinear Sci. and Numerical Simulation* 2007, **8**, 519-526.

15. F. Yang and Y.-P. Zhao, *J. Phys. Chem. C*, 2014, 118, 26859–26865.
16. E. Seyrat and R. A. Hayes, *J. Appl. Phys.* 2001, **90**, 1383.
17. X. Zhang and Y. Cai, *Angewandte Chemie* 2013, **125**, 2345-2348.
18. F. He and S. R. Nugen, *Microfluidics and Nanofluidics* 2014, **16**, 879-886.
19. N. Yang, X. Liu, X. Zhang, B. Lin, H. Yin, Z. Kou, Y. Ding and J. Zhu, *Sensors and Actuators A,* 2014, **219**, 6–12.
20. I. F. Guha, J. Kedzierski and B. Abedian, *Appl. Phys. Lett*. 2011, 99, 024105.
21. M. Dhindsa, S. Kuiper and J. Heikenfeld, Reliable and low-voltage electrowetting on thin parylene film, *Thin Solid Films* 2011, **519**, 3346-51.
22. Y.-Y. Lin, R. D. Evans, E. Welch, B.-N. Hsu, A. C. Madison and R. B. Fair *Sensors Actuators B* 2010, **150**, 465-470.
23. P. T. C. Lee, Ch.-W. Chiu T.-M. Le, T.-Y. Chang, M.-T. Wu, W.-Y. Cheng, Sh.-W. Kuo and J.-J. Lin, *ACS Appl. Mater. Interfaces*, 2013, **5**, 5914–5920.
24. E. Bormashenko, R. Pogreb, Ye. Bormashenko, R. Grynyov and O. Gendelman, *Appl. Phys. Lett*. 2014, **104**, 171601.
25. Ch. Hao, Y. Liu, X. Chen, Y. He, Q. Li, K. Y. Li and Z. Wang, *Scientific Reports*, 2014, **4**, 6846.
26. E. Bormashenko, R. Pogreb, O. Stanevsky, Y. Bormashenko, Y. Socol and O. Gendelman, *Polymers Adv. Techn*. 2005, **16**, 299-304.
27. E. Bormashenko, A. Malkin, A. Musin, Y. Bormashenko, G. Whyman, N. Litvak, Z. Barkay and V. Machavariani, *Macromol. Chem. Physics* 2008, **209**, 567-576.
28. L. Xue, J. Zhang and Y. Han , *Prog. Polym. Sci*. 2012 , **37** , 564 .
29. M. Hernández-Guerrero and M. H. Stenzel, *Polym. Chem*. 2012, **3**, 563.
30. Ed. Bormashenko, S. Balter and D. Aurbach, *Macromol. Chem. Phys*. 2012, **213**, 1742−1747.
31. P. Than, L. Prezosi, D. D. Joseph and M. Arney, *J. Colloid Interface Sci*. 1988, **124,** 552–559.

32. E. Bormashenko, A. Musin, Y. Bormashenko, G. Whyman, R. Pogreb and O. Gendelman, *Macromol. Chem. Phys*. 2007, **208**, 702–709.

33. D. Smith, R. Dhiman, S. Anand, E. Reza-Garduno, R. E. Cohen, G. H. McKinley and K. K. Varanasi, *Soft Matter* 2013, **9**, 1772-1780.

34. S. Anand, A.T. Paxson, R. Dhiman, J. D. Smith and K. K. Varanasi, *ACS Nano* 2012, **6**, 10122-10129.

35. V. Multanen, G. Chaniel, R. Grynyov, R. Y. Loew, N. K. Siany and Ed. Bormashenko, *Colloids and Surfaces A* 2014, **461**, 225–230.

36. Erbil H. Y. *Surface Chemistry of Solid and Liquid Interfaces*, Blackwell, Oxford, 2006.

37. J. N. Israelachvili, *Intermolecular and Surface Forces*, Third Edition, Elsevier, Amsterdam, 2011.

38. P. G. de Gennes, F. Brochard-Wyart and D. Quéré, *Capillarity and Wetting Phenomena*, Springer: Berlin. (2003).

39. E. Bormashenko, *Wetting of Real Surfaces*, de Gruyter, 2013, Berlin.

40. Gelfand I.M and Fomin S. V. *Calculus of Variations*, Dover, 2000.

41. F. Mugele and J.-C. Baret, 2005, *J. Phys.: Condens. Matter* **17,** R705

42. E. Bormashenko, *Math. Model. Nat. Phenom*. 2012, 7, 1–5.

43. E. Bormashenko, *Chem. Phys. Lett*. 2014, **599**, 139–141.

44. F. Li and F. Mugele, *Appl. Phys. Lett*. 2008, **92**, 244108.

45. H. J. J. Verheijen and M. W. J. Prins, *Langmuir* 1999, **15**, 6616-6620.

46. P. Kim, M. J. Kreder, J. Alvarenga and J. Aizenberg, *Nano Lett*. 2013, **13**, 1793-1799.

47. C. Shillingford, N. MacCallum, T.-S. Wong, P. Kim and J. Aizenberg, *Nanotechnology* 2014, **25**, 014019.

48. T.-S. Wong, S. H. Kang, S. K. Y. Tang, E. J. Smythe, B. D. Hatton, A. Grinthal and J. Aizenberg, *Nature* 2011, **477**, 443-447.

49. M. Nosonovsky, *Nature* 2011, **477**, 412-413.

50. St. Sunny, N. Vogel, C. Howell, T. L. Vu and J. Aizenberg, *Adv. Funct. Mater*. 2014, **24**, 6658–6667.

51. R. Tadmor, *Langmuir* 2004, **20**, 7659-7664.

52. M. Nosonovsky, *J. Chem. Phys*. 2007, **126**, 224701.

53. Y. Chernyak, *J. Chem. Eng. Data*, 2006, **51**, 416-418.

54. R. Payne and I. E. Theodorou, *J. Phys. Chem*. 1972, **76**, 2892–2900.

55. S. Arscott, *Scientific Rep*. 2011, **1**, 184.

56. H. Shintaku, Y. Tatara and S. Kawano, *J. Fluid Sci. Tech*., 2009, **4**, 636-647.

57. V. Peykov, A. Quinn and J. Ralston, *Colloid Polymer Sci*. 2000, **278**, 789-793.

58. L. D. Landau and E. M. Lifshitz, *Fluid Mechanics*, (Volume 6 of A Course of Theoretical Physics), Butterworth-Heinemann, Oxford, 1987.

59. A. Staicu and F. Mugele, *Phys. Rev. Lett.* 2006, **97**, 167801.

60. M. Khodayari, J Carballo and N. B. Crane, *Mater. Lett*. 2012, **69**, 96-99.

Table 1. Physical properties of the silicone oil used in the investigation.

Oil	Viscosity, η, Pa×s	Surface tension, γ_{oil}, mJ/m^2	Interface tension, $\gamma_{oil/water}$ mJ/m^2	Density, ρ, 10^3 kg/m^3	Dielectric constant, ε
Silicone oil	0.05	21	23-24	0.963	2.5

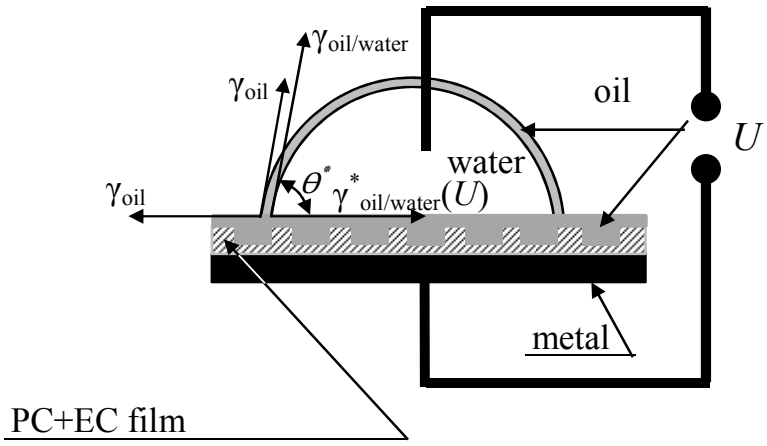

Fig. 1a. EWOLF scheme exploiting a lubricated honeycomb polymer layer as an insulating layer. The balance of interfacial forces is shown.

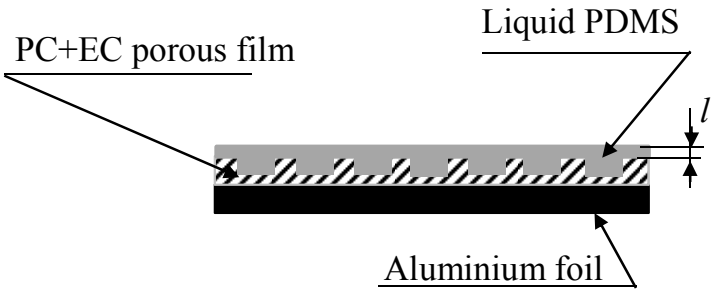

Fig. 1b. Scheme of the electrode used in the EWOLF scheme.

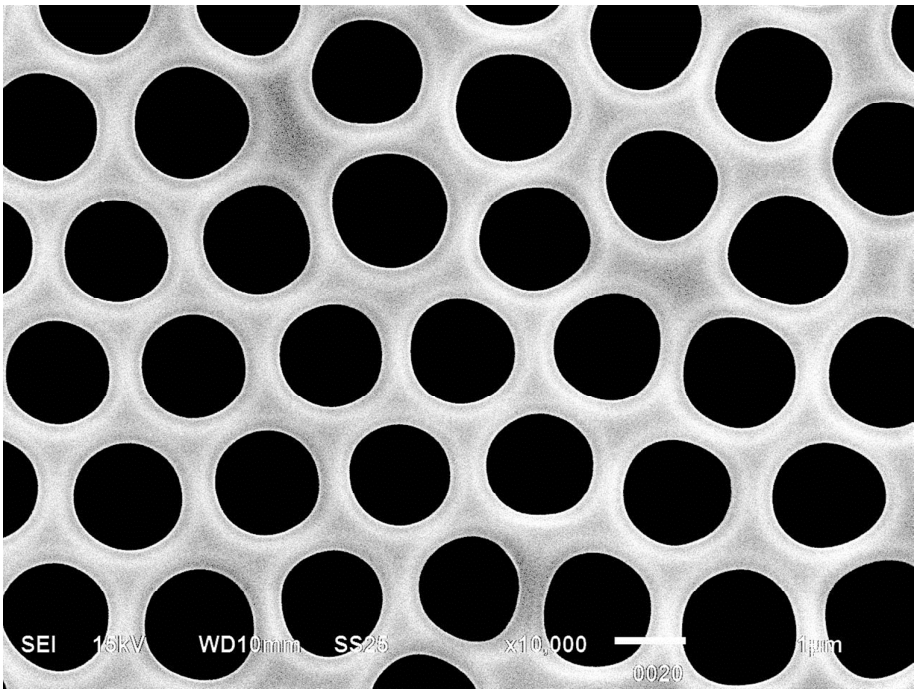

Fig. 2. Composite honeycomb coating built from Polycarbonate and Ethylene Carbonate, deposited on Al plain electrodes obtained with "breath-figures" self-assembly, carried out in a humid atmosphere. Scale bar is 1 μm.

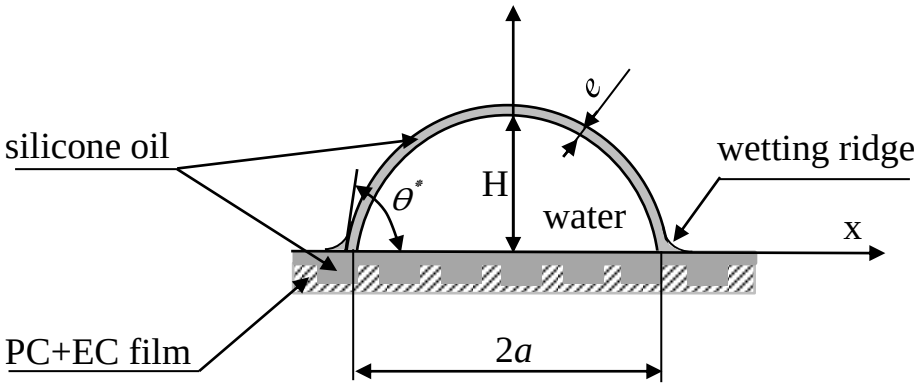

Fig. 3. Parameters of the wetting regime for water droplets deposited on the silicone oil layer. θ^* is the apparent contact angle.

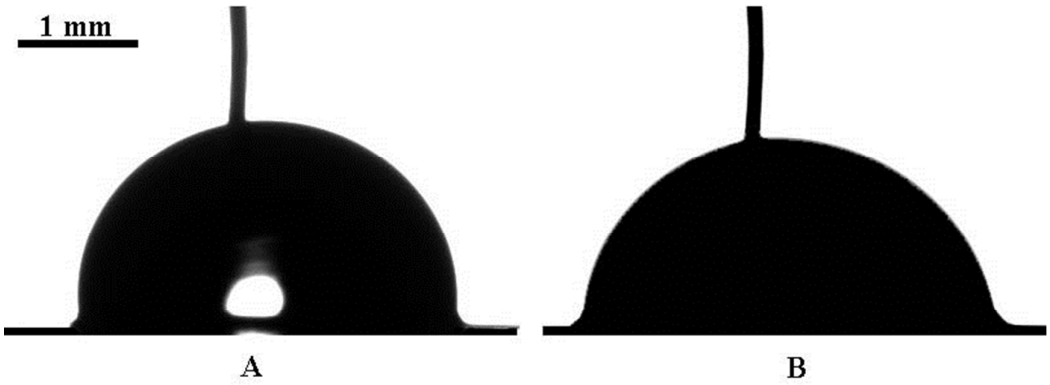

Fig. 4. Electrowetting of silicone oil-lubricated PC+EC substrates. Volume of the water droplet is 8 µl. (a) *U*=0V; (b) *U*=55V.

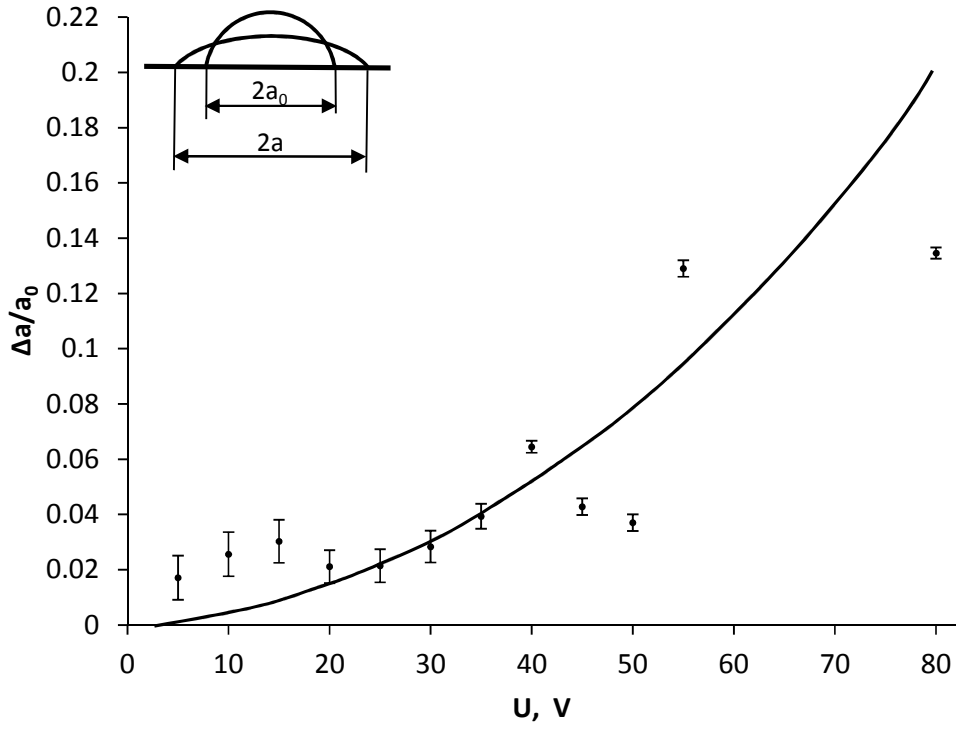

Fig. 5. Relative maximal displacement of the triple line $\Delta a / a_0$ vs. applied DC voltage U for the EWOLF scheme studied in the investigation. Solid line represents the fitting of the experimental data by the function, given by Exps. 10, 12.

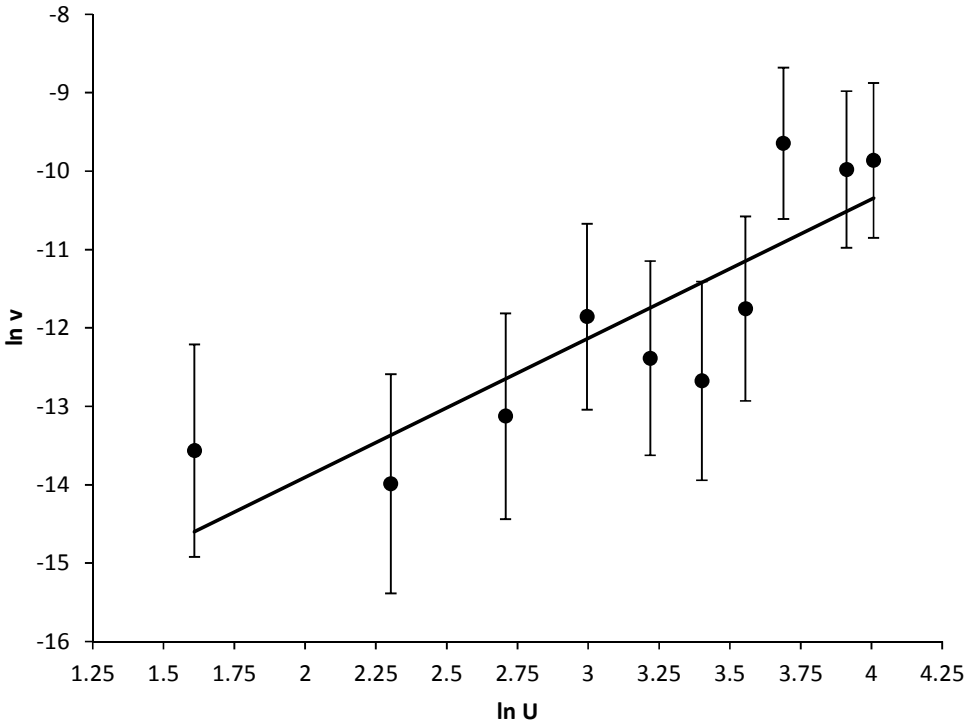

Fig. 6. Average velocity of the triple line *v* (m/s) vs. applied voltage *U* (V) for the EWOLF scheme. The best fitting is presented by the straight line with a slope of 1.8, represented by the solid line.